

# Mechanism of Fucoxanthin on Ferroptosis of Human Erythroleukemia Cells Via the TFR1/SLC7A11/GPX4 Signaling Pathway

Bi Wang<sup>1</sup>, Siyu Wang<sup>2</sup>, Haofei Du<sup>3</sup>, Ziyang Yang<sup>4</sup>, Xiuqiang Zhang<sup>5</sup>,  
Caisheng Wang<sup>6\*</sup>, Haomiao Ding<sup>7\*</sup>

<sup>1,2,3,4,6,7</sup>College of Biological and Environmental Sciences, Zhejiang Wanli University, 8 Qianhu South Road, Ningbo, 315100, China

<sup>5</sup>The First Affiliated Hospital of Ningbo University, 247 Renmin Road, Ningbo, 315000, China

<sup>1</sup>wangbi1031@163.com, <sup>2</sup>Wangsiyu9264@163.com, <sup>3</sup>youzanzizwu@163.com, <sup>4</sup>3529516734@qq.com,

<sup>5</sup>zhangxiuqiang75@163.com, <sup>6</sup>wangcs0528@163.com, <sup>7</sup>dinghm@zwu.edu.cn

\*Correspondence Author

**Abstract:** ***Background:** Fucoxanthin (Fx) is a natural carotenoid gaining widespread interest for its anticancer effects. However, the mechanism by which Fx treats leukemia remains unclear. Here, we studied the mechanism of Fx-induced ferroptosis in human erythroleukemia (HEL) cells. **Methods:** HEL cell viability after Fx treatment was assessed using an MTT assay. Mitochondrial membrane potential (MMP) and cell cycle distribution of HEL cells were determined using flow cytometry. Fucoxanthin's effect on reactive oxygen species (ROS), iron and ferrous ions in HEL cells was measured using assay kits. Expression levels of relevant proteins in HEL cells were assessed through western blot analysis. Molecular docking was performed to validate the interactions. **Results:** Fx significantly inhibited HEL cell viability both dose- and time-dependently. As the Fx concentration increased, the proportion of cells in the G0/G1 phase significantly increased, and MMP and cells in the S phase were notably decreased. Fx markedly promoted ROS, iron and ferrous ion expression levels; reduced GPX4 and SCL7A11 expression levels, and increased p53 and TFR1 expression levels. Molecular docking analysis revealed that the binding energy between Fx and GPX4, SCL7A11, p53 and TFR1 was less than  $-5$  kcal/mol, primarily through hydrogen bonding at the enzyme's active site. **Conclusion:** Fx-induced ferroptosis of HEL cells may be related to activation of the TFR1/SLC7A11/GPX4 signaling pathway.*

**Keywords:** Fucoxanthin, Human erythroleukemia cell, Ferroptosis, Reactive oxygen species, Cell cycle, TFR1/SLC7A11/GPX4 signaling pathway.

## 1. Introduction

Leukemia, a highly aggressive hematological malignancy, is the most malignant blood-related disorder, characterized by challenging treatment modalities and a propensity for relapse [1]. The latest childhood tumor surveillance report revealed leukemia to be the most prevalent serious disease in the pediatric population [2, 3]. Acute lymphoblastic leukemia (ALL), a subtype of leukemia, predominantly affects children aged 0–9 years, comprising approximately 70% of leukemia cases in this demographic [4]. Clinical manifestations include bleeding, anemia, and widespread infiltration of leukemia cells in organs, posing a significant threat to the health of affected children [5]. Current clinical treatment approaches for ALL encompass hematopoietic stem cell transplantation, chemotherapy, radiotherapy, and immunotherapy-targeting drugs [6-8]. Although chemotherapy is the primary treatment modality, curing patients with ALL is challenging after initial treatment and often leads to relapse. Therefore, exploration of new treatment methods and targets is crucial for improving patient compliance and quality of life.

In recent years, the application of natural products in cancer treatment has gained prominence [9]. Moreover, reutilization of natural products has emerged as an alternative approach in anticancer drug development, significantly reducing development timelines and enhancing therapeutic opportunities for patients with leukemia.

Fucoxanthin (Fx) is a naturally occurring carotenoid widely

found in algae, marine phytoplankton, aquatic mollusks, and invertebrates [10]. Fx possesses diverse biological activities such as immune function enhancement, nutritional fortification, and antioxidant, anti-aging, anti-obesity, blood sugar-regulating, and anti-inflammatory effects [11, 12]. Additionally, Fx exhibits potent antitumor activity against skin cancer, leukemia, and tongue carcinoma, among others [13]. The modes of cell death generally include programmed cell death (PCD) and non-programmed cell death (NPCD). PCD is mainly thought to include apoptosis, necroptosis, pyroptosis and autophagy. NPCD includes paraptosis, mitotic catastrophe and oncosis. Fx has been shown to increase cytotoxicity against leukemia K562 cells and decrease proliferation of leukemia TK6 cells [14]. However, few studies have reported Fx's ferroptosis mechanism against ALL.

Ferroptosis is a form of iron-dependent programmed cell death mediated by lipid peroxidation [15]. The process of cell ferroptosis involves iron metabolism, regulation by reactive oxygen species (ROS), and lipid metabolism [16]. Iron is an essential trace element in eukaryotes, playing various roles in oxygen transport, ATP generation, and DNA synthesis [17]. Proper regulation of cellular iron homeostasis is critical for maintaining normal cellular functions. Extracellular iron, in the form of  $Fe^{3+}$ , binds to transferrin receptor protein 1 (TFR1) and enters cells. Subsequently, it is reduced to  $Fe^{2+}$  by six-segment transmembrane epithelial antigen of prostate 3 (STEAP3) and transported into the cytoplasmic labile iron pool by divalent metal-ion transporter-1 (DMT1). Excess

intracellular  $\text{Fe}^{2+}$  catalyzes the Fenton reaction, generating free  $\text{Fe}^{3+}$  hydroxyl radicals and abundant hydrogen peroxide, thus disrupting the cell's antioxidant system [18]. Additionally, the cystine-glutamate antiporter system (System Xc<sup>-</sup>) on the cell membrane, which is crucial for the cellular antioxidant system, exchanges intracellular glutamate with extracellular cysteine. Upon entering cells, nicotinamide adenine dinucleotide phosphate (NADPH) reduces cystine to cysteine and further combines with glycine and glutamate to synthesize glutathione (GSH), reducing intracellular ROS levels [19]. Inhibiting System Xc<sup>-</sup> reduces GSH synthesis, causing a massive accumulation of ROS and disrupting the cell's antioxidant system. Accumulated ROS directly reacts with polyunsaturated fatty acid-phospholipids (PUFA-PL) on the cell membrane, forming lipid hydroperoxides and subsequently lipid peroxides. Moreover, lipoxygenases directly catalyze lipid hydroperoxides [20]. The massive accumulation of lipid peroxides ultimately leads to cell membrane rupture and ferroptosis.

Fx promotes ROS production and inhibits tumor cell growth, and elevated lipid ROS levels are characteristic of ferroptosis [21]. However, the mechanism by which Fx induces ferroptosis in patients with ALL remains unreported, and its precise molecular mechanism requires further study. Here, we used human erythroleukemia (HEL) cells as cellular models and used flow cytometry, fluorescence quantitative PCR, and western blot analysis to investigate the impact and mechanisms of Fx on HEL cell death. Our results help better explain Fx's antitumor mechanisms and support Fx as a potential anticancer drug by modulating cellular ferroptosis, thus presenting a promising novel therapeutic strategy for ALL.

## 2. Material and Methods

### 2.1 Cell Cultures

HEL cells were procured from the Cell Culture Center of the Chinese Academy of Sciences, suspended in RPMI-1640 complete medium containing 10% fetal bovine serum and 1% penicillin-streptomycin (dual-antibiotic; Solarbio, Beijing, China), and cultured at 37°C in a 5% CO<sub>2</sub> incubator.

### 2.2 MTT Assay for Cell Viability

HEL cells were seeded in a 96-well plate at  $5 \times 10^4$  cells per well and cultured for 24 hours. After incubation, 0 (control), 1, 2, 3, 4, 5, 6, 7, 8, 9, and 10  $\mu\text{g}/\text{mL}$  of Fx were added to each well, with five replicates per concentration. A blank culture medium group was also included. After drug exposure for 12, 24, 36, or 48 hours, 10  $\mu\text{L}$  MTT solution (Solarbio) was added to each well, and the cells were cultured for another 4 hours. Absorbance was measured at 570 nm using a microplate reader, and relative cell viability was calculated as follows: relative cell viability (%) = (experimental group A<sub>570</sub> - blank culture medium group A<sub>570</sub>) / (control group A<sub>570</sub> - blank culture medium group A<sub>570</sub>)  $\times$  100%. The experiment was repeated at least three times.

### 2.3 Detection of Mitochondrial Membrane Potential (MMP)

HEL cells were seeded in 6-well plates at  $5 \times 10^4$  cells/mL, 2 mL per well, and cultured for 24 hours. Cells were treated with 0 (control), 3, 6, and 9  $\mu\text{g}/\text{mL}$  Fx, with three replicates per group. After 48 hours of treatment, cells were collected, and JC-1 working solution (BD, Tokyo, Japan) was added and incubated for 20 minutes at 37°C. After washing twice with phosphate-buffered saline (PBS), flow cytometry (BD FACSVerser, Franklin Lakes, NJ, USA) was used to detect the MMP ( $\Delta\psi\text{m}$ ) using FlowJo software, with the ratio of JC-1 red fluorescence to green fluorescence representing the MMP. The fluorescence signals were also measured and recorded using fluorescence microscopy.

### 2.4 Cell Cycle Analysis

Cell cycle changes were determined using DNA content analysis. HEL cells were seeded in 6-well plates at  $5 \times 10^4$  cells/mL, 2 mL per well, and cultured for 24 hours. Cells were treated with 0 (control), 3, 6, and 9  $\mu\text{g}/\text{mL}$  Fx, with three replicates per group. After 48 hours of treatment, cells were collected, washed with twice PBS, fixed with 70% precooled ethanol, and stored overnight at 4°C. After washing with PBS, RNase A (BD, Tokyo, Japan) was added for a 30-minute incubation at 37°C, followed by propidium iodide (PI) staining at room temperature for 30 minutes. Flow cytometry was used to detect the cell cycle. FlowJo software (Tree Star, Ashland, Oregon, USA) was used for the analysis, representing cell cycle arrest based on the difference in fluorescence values.

### 2.5 PCD Detection

HEL cells were seeded in 6-well plates at  $5 \times 10^4$  cells/mL, 2 mL per well, and cultured for 24 hours. Cells were treated with 0 (control), 3, 6, and 9  $\mu\text{g}/\text{mL}$  Fx, with three replicates per group. After 48 hours of treatment, cells were collected, washed with twice PBS, and incubated with 0.1 mL of 1 $\times$  binding buffer, PI, and Annexin-V FITC (BD, Tokyo, Japan) in the dark for 15 minutes. After adding 0.4 mL of 1 $\times$  binding buffer, the mixture was thoroughly mixed, and flow cytometry was used to detect and analyze the PCD using FlowJo software. After 48 hours of treatment, cells were collected, and TUNEL assays were performed according to the instructions in the kits (Abbkine, Wuhan, China). Fluorescence images were captured from random fields at 200 $\times$  magnification.

### 2.6 Detection of Cellular ROS

HEL cells were seeded in 6-well plates at  $5 \times 10^4$  cells/mL, 2 mL per well, and cultured for 24 hours. Cells were then treated with 0 (control), 3, 6, and 9  $\mu\text{g}/\text{mL}$  Fx, with three replicates per group. After 48 hours of treatment, cells were collected, resuspended with freshly prepared DCFH-DA fluorescent probe solution (Solarbio), and incubated at 37°C for 30 minutes. After washing twice with culture medium and resuspending the cells in PBS, flow cytometry was used to detect cellular ROS levels, represented by the mean fluorescence intensity.

### 2.7 Detection of Ferroptosis-related Indicators

HEL cells were seeded in 6-well plates at  $5 \times 10^4$  cells/mL, 2

mL per well, and cultured for 24 hours. Cells were treated with 0 (control), 3, 6, and 9  $\mu\text{g}/\text{mL}$  Fx, with three replicates per group. After 48 hours of treatment, cells were collected, and assays for glutathione (GSH), malondialdehyde (MDA), iron and ferrous ions were performed according to the instructions in the kits (Solarbio). Absorbance was measured using a microplate reader.

## 2.8 qPCR for Gene Expression

HEL cells were seeded in 6-well plates at  $5 \times 10^4$  cells/mL, 2 mL per well, and cultured for 24 hours. Cells were treated with 0 (control), 3, 6, and 9  $\mu\text{g}/\text{mL}$  Fx, with three replicates per group. After 48 hours of treatment, total RNA was extracted using TRIzol reagent (Tokyo, Japan). Reverse transcription was performed to obtain cDNA, followed by real-time fluorescence quantitative gene detection (RT-qPCR). The qPCR reaction conditions were 95°C for 10 min, 95°C for 30 s, 55°C for 30 s, and 72°C for 15 s, for 40 cycles. Table 1 lists the primers used.  $\beta$ -actin was used as the reference gene.

**Table 1: Primers used for RT-qPCR.**

Genes	Sense Primers (5'-3')	Antisense Primers (3'-5')
<i>p53</i>	GCGTGTGGAGTATTTGGA TGAC	AGTGTGATGATGGTGAG GATGG
<i>TFR1</i>	AACTCAGCAAAGTCTGGC GT	GACCCCAATACACCGCA TA
<i>SLC7A11</i>	TCCTGCTTTGGCTCCAT	ACAGGCGTTTCGTGTGAGG AGA
<i>GPX4</i>	ACAAGAACGGCTGCGTG GTGAA	AGATCGAGGTGTTTCACAC ACCG
<i><math>\beta</math>-actin</i>	CCTGGCACCCAGCACAAAT	GGGCCGGACTCGTCATAC

## 2.9 Western Blot for Protein Levels

HEL cells were seeded in 6-well plates at  $5 \times 10^4$  cells/mL, 2 mL per well, and cultured for 24 hours. Cells were treated with 0 (control), 3, 6, and 9  $\mu\text{g}/\text{mL}$  Fx, with three replicates per group. Cells were lysed with RIPA protein lysis buffer, and the supernatant was collected. SDS-PAGE electrophoresis was performed by adding protein loading buffer to the protein and boiling for 5 minutes at 95°C to prepare the samples. A 12% separating gel and 6% concentrating gel were used for electrophoresis at 100 V for 90 minutes to separate the protein samples. Transblotting and blocking were performed using an NC membrane (Millipore Co., Billerica, MA, USA). The SDS-PAGE gel was placed on the transblotting apparatus, and electrophoresis was performed in an ice-water bath at 90 V for 100 minutes to transfer the proteins from the gel to the NC membrane. The membrane was then blocked with 1% defatted milk at room temperature for 1 hour. SLC7A11 (ABclonal Technology, Wuhan, China), GPX4 (ABclonal Technology), TFR1 (ABclonal Technology) and p53 (ABclonal Technology) antibodies were incubated with the primary antibody (1:1000 dilution) overnight at 4°C. The secondary antibody (1:5000 dilution; ABclonal Technology) was incubated at room temperature for 2 hours. Imaging was performed using an ECL detection kit, and images were captured using a gel imaging system.

## 2.10 Molecular Docking

The Fx chemical structure was drawn using ChemDraw 19.0 software and subjected to energy minimization using Chem3D 14.0 software. The TFR1 protein structure (PDB ID:

7ZQS), SLC7A11 protein structure (PDB ID: 7P9U), GPX4 protein structure (PDB ID: 5H5Q), p53 protein structure (PDB ID: 3KMD) were retrieved from the Protein Data Bank (<https://www.rcsb.org/>) and saved in pdb format. Pymol 2.5.2 was used to remove water molecules and eliminate modified ligands. AutoDock Tools 1.5.7 was used to convert Fx and TFR1 or SLC7A11 or GPX4 or p53 protein into pdbqt format for molecular docking. LigPlus 2.5.5 was used to analyze hydrogen bonding, hydrophobic interactions, and other forces between the ligand and protein.

## 2.11 Statistical Methods

Statistical analyses were performed using ImageJ and FlowJo software. All experiments were conducted in triplicate. Data are presented as means  $\pm$  standard deviation unless otherwise indicated. Differences between two groups were analyzed using Student's t-tests; comparisons among multiple groups were made using analysis of variance (ANOVA). Statistical analyses were carried out using GraphPad Prism 8 software. Thresholds for statistical significance were defined as  $*p < 0.05$  and  $**p < 0.01$ .

## 3. Results

### 3.1 Fx Reduced HEL Cell Viability

To investigate whether Fx reduces HEL cell viability, various Fx concentrations were used to treat HEL cells for varying durations, and cells were subjected to MTT assay (Figure 1). Regardless of the treatment duration (12, 24, 36, or 48 h), low concentrations (0-2  $\mu\text{g}/\text{mL}$ ) of Fx did not significantly inhibit HEL cell viability. Medium concentrations (3-6  $\mu\text{g}/\text{mL}$ ) significantly or markedly inhibited cell viability concentration-dependently, reducing it to  $<90\%$ . High concentrations (7-10  $\mu\text{g}/\text{mL}$ ) significantly inhibited HEL cell viability, which dropped to  $<50\%$  after 36 hours, demonstrating clear time dependency.

### 3.2 Fx Promoted PCD in HEL Cells

PCD induction by Fx was assessed using Annexin-V/PI staining. In the control group, the PCD rate of HEL cells was 5.81%. At 3  $\mu\text{g}/\text{mL}$  Fx, the PCD rate increased to 11.44%; at 6  $\mu\text{g}/\text{mL}$ , the PCD rate significantly increased to 59.03%; and at 9  $\mu\text{g}/\text{mL}$ , the PCD rate of HEL cells reached 84.90%. As the Fx concentration increased, the PCD, early PCD, and late PCD rates of HEL cells increased (Figure 2a). Thus, Fx effectively promoted early PCD in HEL cells, but late PCD was not obvious. To determine whether the late programmed death of HEL cells is affected by Fx, we performed TUNEL fluorescence staining experiments. The ratio of green to blue fluorescent cells represents the proportion of late programmed death cells in all cells. As shown in Figure 2b, in the absence of Fx, late programmed death accounted for 2.15% of total HEL cells. After 0, 3, 6, and 9  $\mu\text{g}/\text{mL}$  Fx treatment, the proportion increased to 4.28%, 5.23%, and 11.67%, respectively.

### 3.3 Fx Promoted MMP Loss and Cell Cycle Arrest in HEL Cells

MMP loss is a hallmark event of early apoptosis, usually

occurring at the onset of PCD. Compared with normal cells, tumor cells typically exhibit hyperpolarized MMP. JC-1 staining was used to detect changes in the MMP of HEL cells (Figure 3a). Fx promoted MMP loss in HEL cells concentration-dependently. In healthy cells with high MMP, JC-1 forms complexes called J-aggregates, emitting red/orange fluorescence. Decreased MMP leads to emission of green fluorescence by JC-1 monomers. Flow cytometry results showed a significant decrease in the red/green fluorescence ratio in HEL cells treated with different Fx concentrations. Particularly, Fx at 9  $\mu\text{g/mL}$  induced a significant loss of MMP, with a rate of 70.71%.

To further investigate the effect of Fx on the HEL cell cycle, PI staining was used with flow cytometry. Compared with the control group, the proportion of cells in G1 phase significantly increased, and that of cells in S phase significantly decreased as the drug concentration increased, with no significant difference in S phase at 0 and 3  $\mu\text{g/mL}$ . However, at 3 and 6  $\mu\text{g/mL}$ , the proportion of cells in G2 phase significantly decreased (Figure 3b). In summary, Fx significantly arrested HEL cells in G1 phase. Combined with the results of the MMP experiments, we speculate that Fx-induced PCD in HEL cells may be the mechanism of ferroptosis.

### 3.4 Fx Affected Ferroptosis-related Indicators in HEL Cells

Ferroptosis is a form of iron-dependent lipid peroxidation-induced cell death. External stimulation of HEL cells affects MMP, influencing the respiratory chain and leading to ROS generation. Excessive ROS levels induce mitochondrial autophagy. To explore whether oxidative stress causes HEL cell death, the ferrous ion colorimetric method was used to detect changes in cellular iron levels. MDA and GSH assay kits were used to quantitatively analyze intracellular levels of lipid peroxidase and reduced GSH to comprehensively assess cellular iron ions and lipid peroxidation. HEL cells were treated with various FX concentrations to evaluate whether Fx affects ferroptosis in HEL cells. Fx-induced ROS production was detected using an ROS probe (Figure 3). Fx induced ROS production in HEL cells concentration-dependently, with 9  $\mu\text{g/mL}$  of Fx inducing a significant increase in ROS levels (Figure 4a and b). Thus, Fx may promote PCD in tumor cells by triggering oxidative stress. Determination of GSH levels showed that FX treatment at 6 and 9  $\mu\text{g/mL}$  decreased intracellular GSH levels (Figure 4c). Compared with the control group, 3, 6, and 9  $\mu\text{g/mL}$  of Fx significantly increased the MDA, ferrous ions, and iron ions in HEL cells (Figure 4d-f). Therefore, medium to high doses of Fx induced ferroptosis in HEL cells.

### 3.5 Fx Regulates the SLC7A11/GPX4 Pathway to Induce HEL Cell Death

RT-qPCR was performed to detect the mRNA levels of ferroptosis-related genes in HEL cells. Relative expression levels of GPX4 and SLC7A11 gradually decreased as the Fx concentration increased (Figure 5a and b). In the group treated with 3  $\mu\text{g/mL}$  of Fx, the expression levels of ferroptosis-related genes SLC7A11 and GPX4 were significantly reduced ( $p < 0.05$ ). When the concentration exceeded 3  $\mu\text{g/mL}$ , the expression levels of ferroptosis-related

genes TFR1 and p53 significantly or markedly increased ( $p < 0.05$ ,  $p < 0.01$ ; Figure 5c and d). To further explore the mechanism by which Fx regulates ferroptosis in HEL cells, the expression of ferroptosis-related proteins was examined (Figure 5e). Relative expression levels of GPX4 and SLC7A11 gradually decreased as the Fx concentration decreased, and at 9  $\mu\text{g/mL}$ , the relative expression levels of GPX4 and SLC7A11 significantly decreased ( $p < 0.01$ ; Figure 5f and h). At 9  $\mu\text{g/mL}$  of Fx, the relative expression level of p53 and TFR1 increased extremely significantly ( $p < 0.01$ ; Figure 5i and j). Fx effectively promoted ferroptosis in HEL cells.

### 3.6 Molecular Docking Validation

To explore the relationship between Fx and its target proteins, molecular docking simulations were performed for Fx with SLC7A11, GPX4, p53, and TFR1. Pymol 2.1 software was used to visualize the Fx-target protein complexes, obtaining binding modes that clearly show interacting amino acid residues at the binding site. The molecular docking results (Figure 6) indicate that the binding energy between Fx and SLC7A11 was less than  $-5.81$  kcal/mol, and the binding energy between Fx and GPX4 was less than  $-7.23$  kcal/mol. The binding energy between Fx and TFR1 was less than  $-7.91$  kcal/mol, and the binding energy between Fx and p53 was less than  $-7.3$  kcal/mol, indicating high binding efficiency. Fx formed hydrogen bonds with SLC7A11, which included interactions with LYS-106 (2.1 Å) and PRO-415 (2.2 Å) (Figure 6a). Similarly, Fx formed hydrogen bonds with GPX4 by interacting with ARG-36 (2.1 Å), GLY-111 (2.4 Å), and ASP-34 (2.2 Å) (Figure 6b); with TFR1 by interacting with PHE-298 (1.8 Å, 2.5 Å), LYS-534 (1.9 Å), LEU-566 (1.9 Å), and GLU-533 (2.1 Å, 2.9 Å) (Figure 6c); and with p53 by interacting with THR-102 (1.9 Å) (Figure 6d). Thus, Fx is likely directly associated with the TFR1/SLC7A11/GPX4 pathway (Figure 7).

## 4. Discussion

ALL is one of the most common malignant tumors, and multidrug chemotherapy is the main treatment strategy [22]. The early stages of treatment typically yield significant anticancer effects, particularly in patients with late-stage cancer. However, with prolonged exposure to chemotherapeutic drugs, genetic and epigenetic changes occur in tumor cells, leading to the development of drug-resistant clonal subtypes [23]. Under the high pressure of chemotherapy, these drug-resistant tumor cell lines exhibit enhanced resistance. Despite recent discoveries of new molecular targets and compounds for treating ALL that exhibit lower recurrence rates and higher remission rates, the combination of monoclonal antibodies and chemical drugs in chemical immunotherapy is associated with a poor clinical prognosis due to toxic adverse effects such as cytokine release syndrome, neurotoxicity, and multiorgan dysfunction [24]. Therefore, new compounds with anti-ALL properties should be explored to offer more comprehensive treatment options for ALL.

Natural products are important sources of therapeutic agents and have gained increasing attention in cancer treatment [25, 26]. Fx has demonstrated excellent anti-leukemia activity in

two human leukemia cell lines, K562 and TK6 [14]. Research indicates that Fx acts on multiple targets, regulating the expression of proteins in various signaling pathways and promoting PCD in tumor cells [27]. Cell experiments have shown that Fx effectively inhibits HEL cell viability. The MTT assay determined IC50 values for Fx at 12, 24, 36, and 48 hours, demonstrating dose- and time-dependent effects on HEL cell viability. This suggests that Fx may be a promising drug for treating HEL. PCD-related changes, such as phosphatidylserine externalization, MMP reduction, and cell cycle arrest, were observed using the fluorescent dyes Annexin-V, PI, and JC-1. Ahmed et al. found that Fx induced cell cycle arrest at the G1 phase in MDA-MB-231 and MDA-MB-468 cells. Fx can target VEGF-A and VEGF-C, inhibit cell proliferation and cell migration, and induce cell cycle arrest and apoptosis, the most crucial cellular processes [28]. Flow cytometry analysis revealed that Fx dose-dependently induced G1 phase cell cycle arrest and significantly decreased MMP in HEL cells. Annexin/PI double staining showed a dose-dependent increase in PCD rates, although the proportion of late-stage PCD did not significantly rise. This suggests that Fx promotes HEL cell death through other mechanisms. These results combined with the MMP experimental results suggest that the mechanism by which Fx promotes HEL cell death may involve ferroptosis.

Ferroptosis, primarily caused by intracellular iron accumulation and lipid peroxidation, involves the crucial roles of lipid peroxidation and GSH depletion [29]. This process includes ROS-driven lipid oxidation, ultimately leading to cell damage and membrane rupture. The interplay between lipid peroxidation and ferroptosis is complex, where ROS promotes iron accumulation, and vice versa, enhancing oxidative stress. Excessive iron and lipid peroxidation products (e.g., ROS) can severely damage the cell membrane. Ferroptosis plays different roles in different stages of tumor development, inhibiting cell proliferation and differentiation in cellular homeostasis regulation. Our results showed that ROS levels in HEL cells increased with the Fx concentration. ROS, a group of highly reactive molecules generated during aerobic metabolism, participates in cell signal transduction. Consistent with our findings, another study revealed that bisphenol A treatment downregulated SH-SY5Y cell viability concentration-dependently and increased the ROS levels concentration-dependently [30]. High ROS levels induce cell death by damaging DNA and causing DNA breaks, leading to genomic instability and ultimately inducing cell death [31]. Further experiments revealed that Fx treatment increased lipid peroxidation levels, iron and ferrous ion concentrations, while decreasing GSH levels. Iron ions typically bind to transferrin in the form of trivalent iron, enter the cell through the transferrin channel, and are reduced to divalent iron by the metal reductase, STEAP3, which preferentially forms various iron-binding complexes. When the content of these complexes nears saturation, excess divalent iron accumulates in the cell, forming an unstable iron pool [18]. The free divalent iron in the iron pool participates in the Fenton reaction, which generates ROS represented by hydroxyl radicals. The accumulated ROS oxidizes membrane lipids, resulting in the loss of cell function. GSH, a major nonenzymatic antioxidant in cells, is synthesized from glutamate, cysteine, and glycine. It directly acts as an

antioxidant and serves as a substrate for GPX4 [32]. GPX4 is the only enzyme in cells that reduces lipid peroxides, converting intracellular GSH to glutathione disulfide, and detoxifying toxic lipid peroxides into non-toxic alcohols, accelerating H<sub>2</sub>O<sub>2</sub> decomposition, and preventing and alleviating peroxide-induced damage to cell structures [33]. When GSH is depleted under oxidative stress, GPX4 becomes inactive, and GPX4 downregulation is considered a key feature of ferroptosis [34]. Both qPCR and western blot results indicated a significant concentration-dependent downregulation of GPX4 expression in HEL cells after Fx treatment. Additionally, Terasaki et al. found that dysregulation of signals by TP53, ARID1A, NRAS, and PMS2 mutations might have been mitigated because Fx administration effectively suppressed tumor growth in CRC-PDX mice [35]. Fx's inhibitory effect on tumor cells is also related to its induction of p53 overexpression. p53, encoded by TP53, functions in cells to monitor DNA damage and prompts the cells to respond appropriately. When DNA is damaged, p53 halts the cell cycle, allowing cells to enter the repair state. If the repair is ineffective, p53 induces cell death via apoptosis [36]. p53, known for its regulatory roles in cell proliferation, apoptosis, aging, and metabolism across diverse tissues, appears to play a pivotal role in aggravating biological processes such as epithelial-mesenchymal transition, apoptosis, and cell senescence [37]. p53 can directly bind to the p53-binding elements in the SLC7A11 promoter region, thereby inhibiting SLC7A11 expression and increasing cell sensitivity to ferroptosis [38]. Both qPCR and western blot results indicated a concentration-dependent significant downregulation of SLC7A11 expression in HEL cells after Fx treatment. Upregulated p53 can also upregulate TFR1 expression levels and increase intracellular iron ion contents, and excess iron can generate ROS through the Fenton reaction, leading to ferroptosis [39]. In this study, TFR1 expression levels significantly and dose-dependently increased as the Fx concentration increased. Few studies have systematically investigated ferroptosis by Fx in cancer cells; however, their findings seem consistent with ours. Zhu et al. (2023) showed that Fx inhibited glioblastoma cell survival by triggering ferroptosis, a ferric ion and ROS-dependent cell death, which was blocked by ferrostatin-1 [40]. We conducted molecular docking simulations to further analyze the mechanism of Fx on SLC7A11, GPX4, p53, and TFR1. Fx exhibited strong binding affinity with SLC7A11, GPX4, p53, and TFR1, which was attributed to formation of strong hydrogen bonds between Fx and SLC7A11, GPX4, p53, and TFR1 residues. The hydrogen bond distances were relatively short, facilitating stable interaction between the ligand (Fx) and proteins (SLC7A11, GPX4, p53, and TFR1).

## 5. Conclusion

Our results demonstrated that Fx can reduce HEL cell viability concentration- and time-dependently. Fx induced MMP loss in HEL cells, leading to cell cycle arrest and ferroptosis. The mechanism underlying these effects involves promoting ferroptosis in HEL cells, as evidenced by changes in ROS production, lipid peroxidation, and iron-related proteins and genes. Molecular docking simulations further supported a direct interaction between Fx and SLC7A11, GPX4, p53, and TFR1, key proteins involved in ferroptosis. These findings contribute to our understanding of the

antileukemic effects of Fx and provide a basis for further exploring its therapeutic potential in leukemia treatment.

**Acknowledgements:** Not applicable.

**Author Contributions:** Caisheng Wang and Haomiao Ding contributed to the conception of the study. Bi Wang, Siyu Wang, Haofei Du and Ziyang Yang performed the experiment. Xiuqiang Zhang contributed significantly to the analysis. Bi Wang and Siyu Wang performed the data analysis and wrote the manuscript. Caisheng Wang and Haomiao Ding helped perform the analysis with constructive discussion.

**Funding:** This research was funded by Zhejiang Provincial Top Discipline of Biological Engineering (KF2022010), General Scientific Research Project of Zhejiang Education Department (Y202455066), The Natural Science Foundation of Ningbo City (2023J294, 2024J249).

**Data Availability:** Data will be made available on request.

**Declarations**

**Conflict of interest:** The authors confirm that they have no financial or personal ties to other parties that could be seen as influencing the results presented in this paper.

**Ethical approval** Not applicable.

**Informed consent** Not applicable.

## Figure Legends

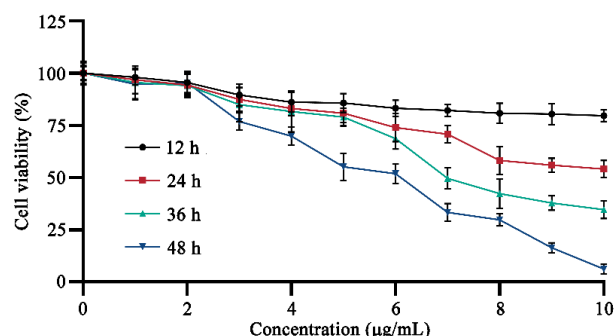


**Figure 1:** Variations in the viability of HEL human erythroleukemia cells over time at different concentrations of Fx. Data are means  $\pm$  SD ( $n=5$ ).

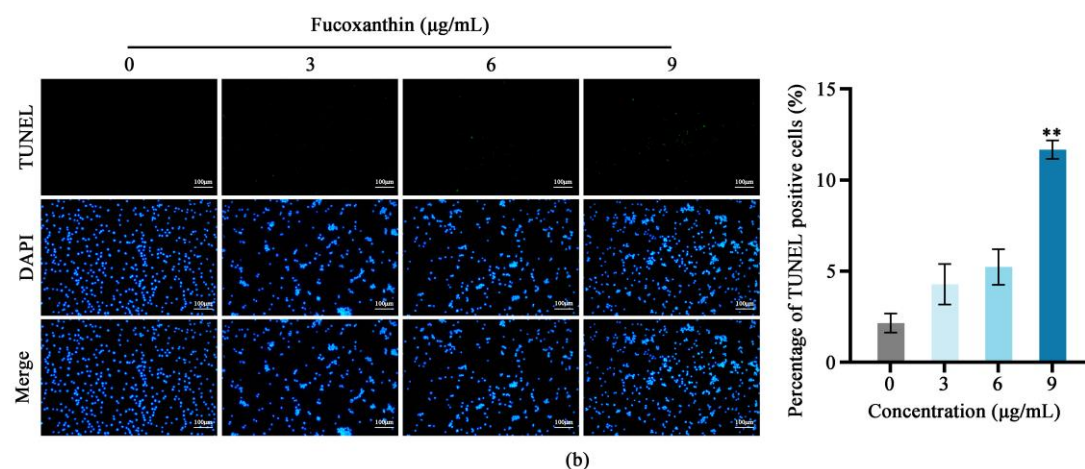
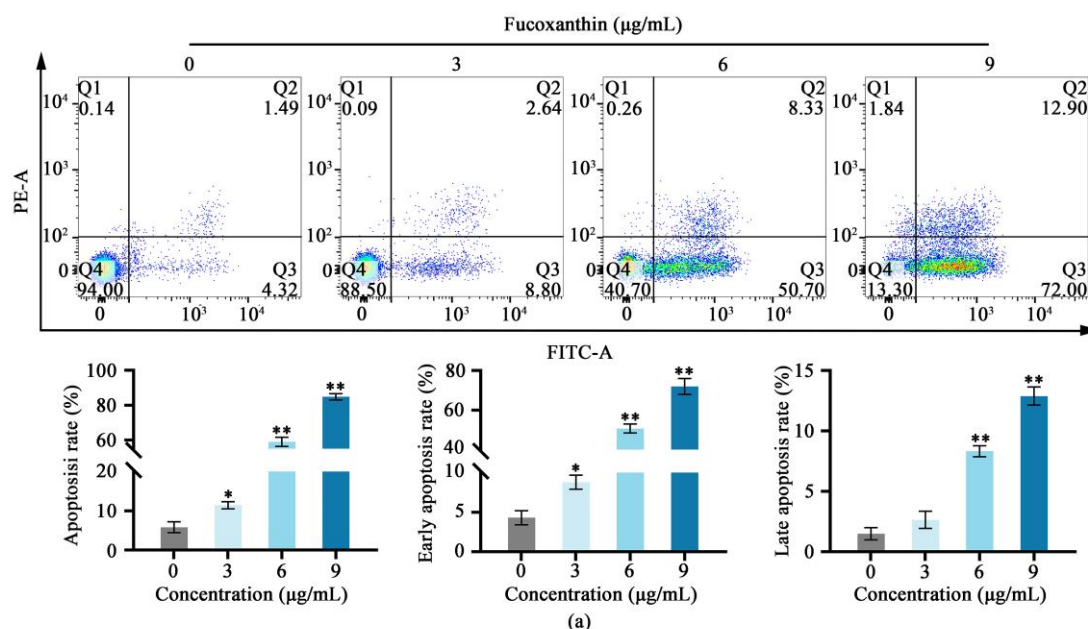


**Figure 2:** Effects of Fx on PCD of HEL cells ( $n=3$ ). (a) Effect of Fx on PCD of HEL cells. Q1: dead cells; Q2: cells in end-stage PCD; Q3: cells undergoing PCD; Q4: viable cells not undergoing PCD. (b) Late PCD of HEL cells treated with Fx was qualitatively and quantitatively assessed by TUNEL fluorescence microscopy. \* and \*\* indicate significant ( $p < 0.05$ ) and extremely significant ( $p < 0.01$ ) differences compared with the control group.

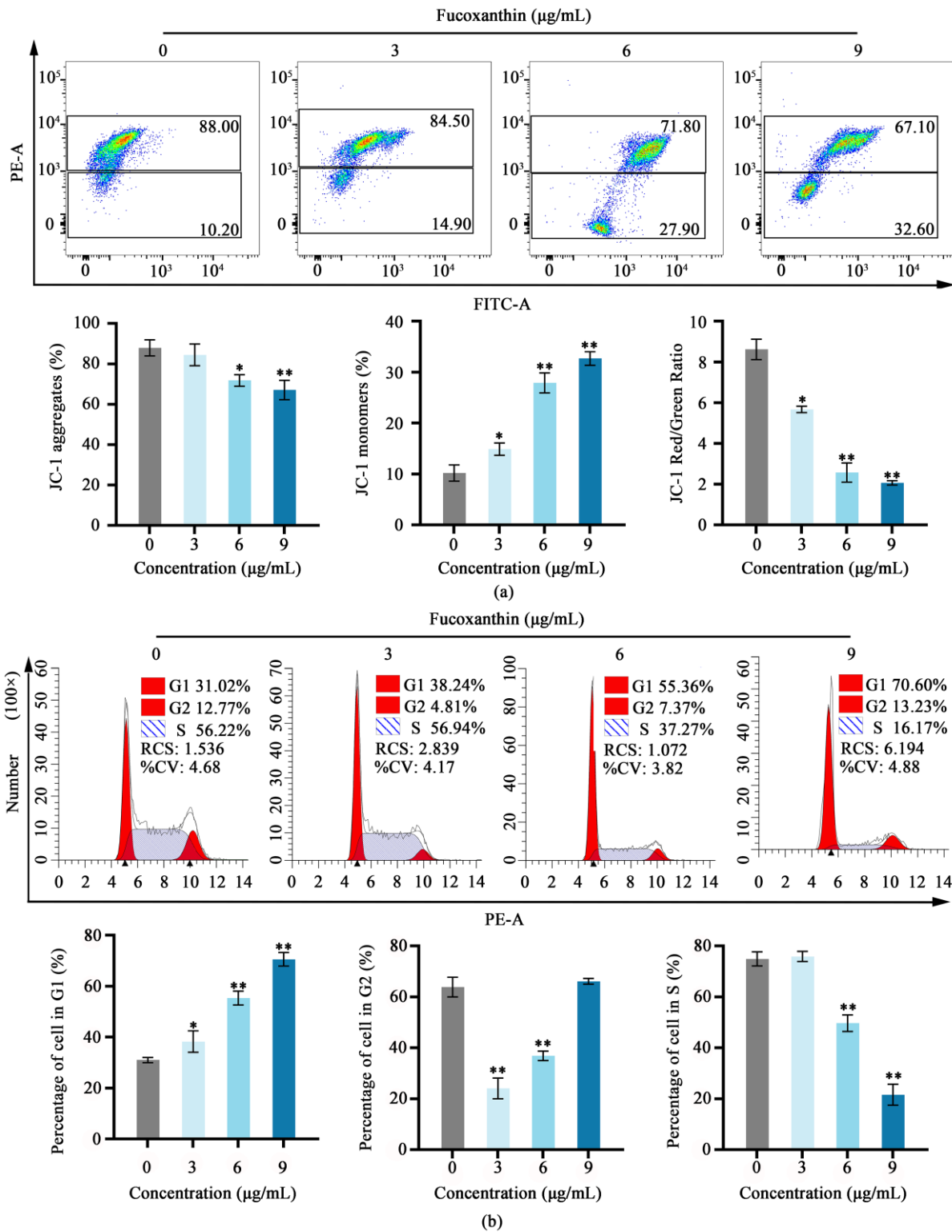


**Figure 3:** Effects of Fx on MMP and cell cycle of HEL cells ( $n=3$ ). (a) Effect of Fx on HEL MMP. (b) Effect of Fx on HEL cell cycle. \* and \*\* indicate significant ( $p < 0.05$ ) and extremely significant ( $p < 0.01$ ) differences compared with the control group.

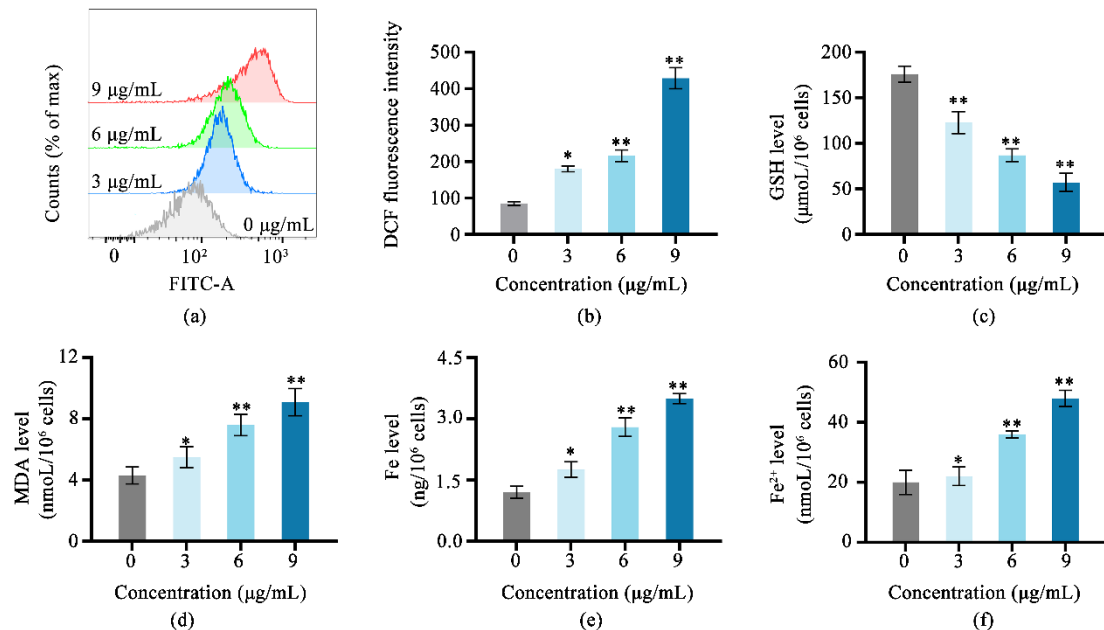


**Figure 4:** Fx-induced ferroptosis in HEL cells ( $n=3$ ). (a) Effects of Fx on ROS in HEL cells. (b) Effects of Fx on levels of dichlorofluorescein fluorescence intensity of ROS in HEL cells. (c) Effects of Fx on GSH levels in HEL cells. (d) Effects of Fx on MDA levels in HEL cells. (e) Effects of Fx on Fe levels in HEL cells. (f) Effects of Fx on Fe<sup>2+</sup> levels in HEL cells. \* and \*\* indicate significant ( $p < 0.05$ ) and extremely significant ( $p < 0.01$ ) differences compared with the control group.

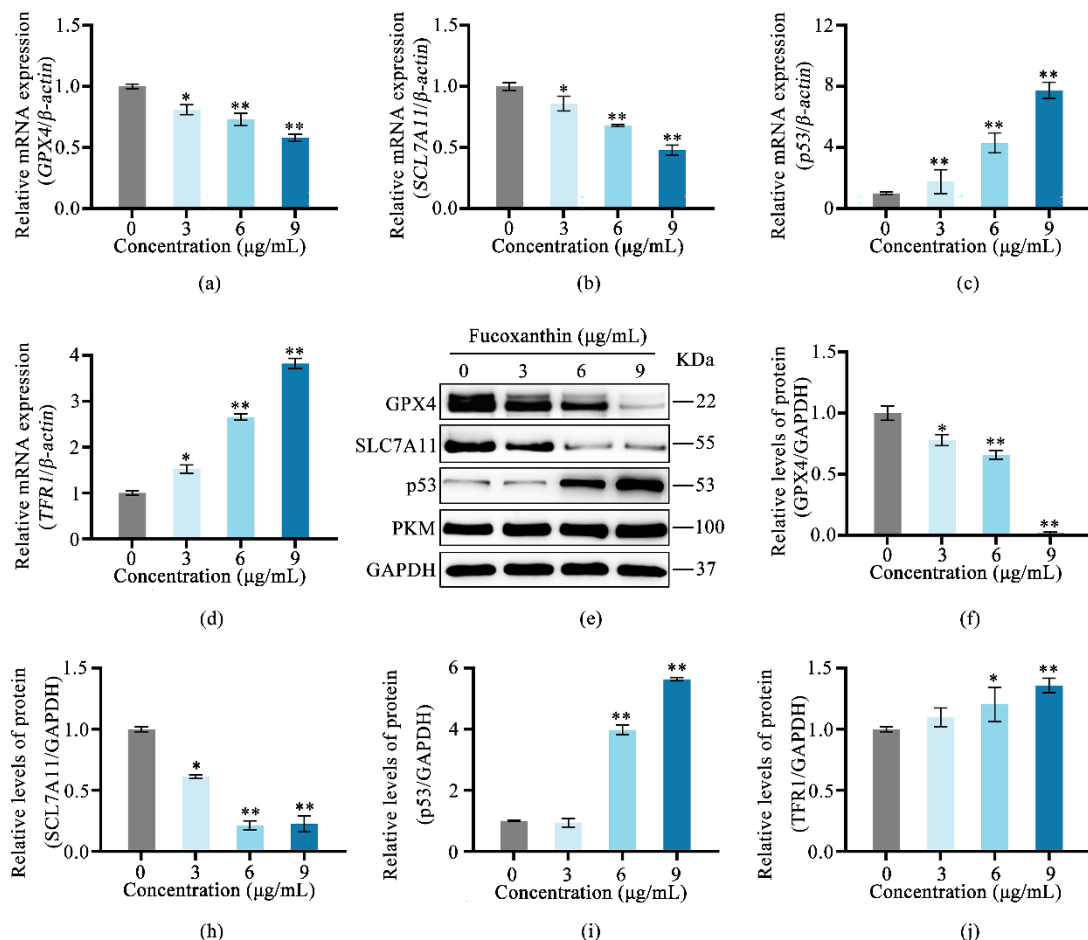


**Figure 5:** Fx-regulated gene and protein expression of TFR1/SLC7A11/GPX4 pathway-induced ferroptosis in HEL cells ( $n=3$ ). (a) Effect of Fx on GPX4 mRNA expression in HEL cells. (b) Effect of Fx on SLC7A11 mRNA expression in HEL cells. (c) Effect of Fx on p53 mRNA expression in HEL cells. (d) Effect of Fx on TFR1 mRNA expression in HEL cells. (e) Protein immunoblotting. (f) Effect of Fx on GPX4 protein expression in HEL cells. (h) Effect of Fx on SLC7A11 protein expression in HEL cells. (i) Effect of Fx on p53 protein expression in HEL cells. (j) Effect of Fx on TFR1 protein expression in HEL cells. \* and \*\* indicate significant ( $p < 0.05$ ) and extremely significant ( $p < 0.01$ ) differences compared with the control group.

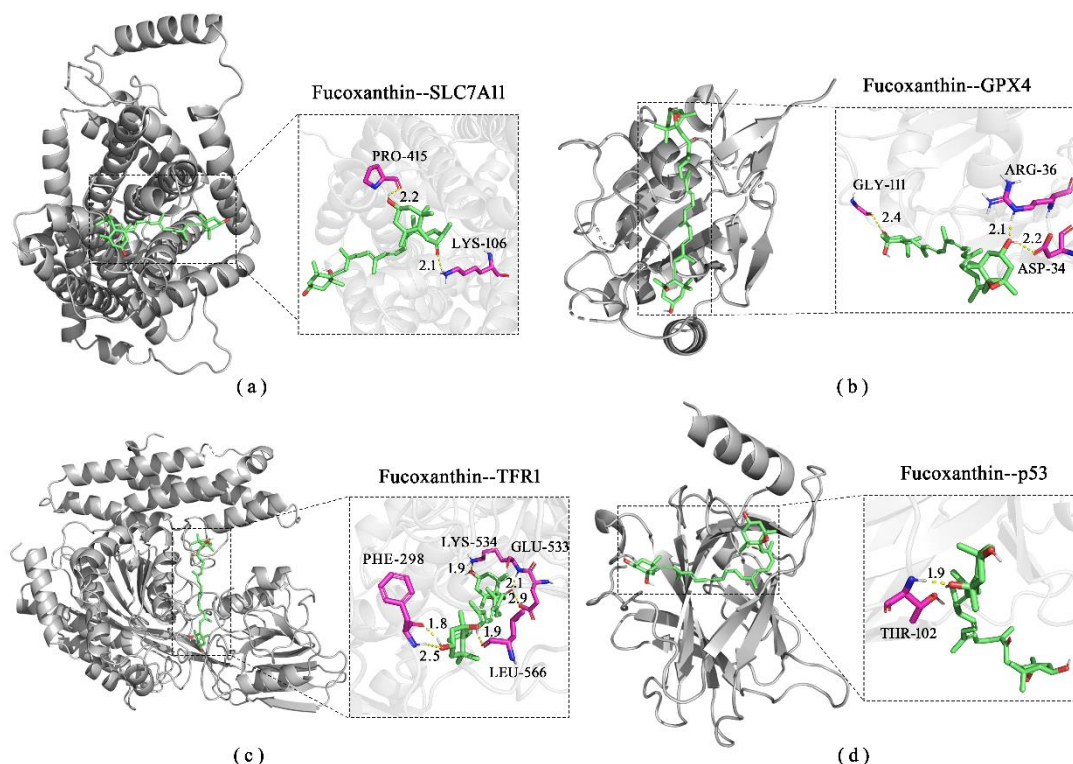


**Figure 6:** Molecular docking of Fx in intervention targets. (a) Molecular docking results between Fx and SLC7A11; (b) Fx and GPX4; (c) Fx and TFR1; and (d) Fx and p53.

## References

- [1] Yankova E, Blackaby W, Albertella M, Rak J, De Braekeleer E, Tsagkogeorga G, Pilka ES, Aspris D, Leggate D, Hendrick AG, Webster NA, Andrews B, Fosbeary R, Guest P, Irigoyen N, Eleftheriou M, Gozdecka M, Dias JML, Bannister AJ, Vick B, Jeremias I, Vassiliou GS, Rausch O, Tzelepis K, Kouzarides T. Small molecule inhibition of METTL3 as a strategy against myeloid leukaemia. *Nature* 2021, 593, 597-601.
- [2] Chiesa R, Georgiadis C, Syed F, Zhan H, Etuk A, Gkazi SA, Preece R, Ottaviano G, Braybrook T, Chu J, Kubat A, Adams S, Thomas R, Gilmour K, O'Connor D, Vora A, Qasim W. Base-edited CAR7 T cells for relapsed T-cell acute lymphoblastic leukemia. *New Engl. J. Med.* 2023, 389, 899-910.
- [3] Inaba H, Mullighan CG. Pediatric acute lymphoblastic leukemia. *Haematologica* 2020, 105, 2524-2539.
- [4] Egan G, Tasian SK. Relapsed pediatric acute myeloid leukaemia: state-of-the-art in 2023. *Haematologica* 2023, 108, 2275-2288.
- [5] Eghbali A, Sadeghian M, Ghasemi A, Afzal RR, Eghbali A, Ghaffari K. Effect of oral silymarin on liver function in pediatric acute lymphoblastic leukemia in the maintenance phase: a double-blind randomized clinical trial. *Front. Pharmacol.* 2024, 15, 1295816.
- [6] Barrios-Palacios D, Organista-Nava J, Baladrán JC, Alarcón-Romero LD, Zubillaga-Guerrero MI, Illades-Aguiar B, Rivas-Alarcón AA, Diaz-Lucas JJ, Gómez-Gómez Y, Leyva-Vázquez MA. The role of miRNAs in childhood acute lymphoblastic leukemia relapse and the associated molecular mechanisms. *Int. J. Mol. Sci.* 2023, 25, 119.
- [7] Testa U, Sica S, Pelosi E, Castelli G, Leone G. CAR-T cell therapy in b-cell acute lymphoblastic leukemia. *Mediterr. J. Hematol. I.* 2024, 16, e2024010.
- [8] Zhang KA, An XZ, Zhu Y, Huang L, Yao XY, Zeng X, Liang SY, Yu J. Netrin-1 inducing antiapoptotic effect of acute myeloid leukemia cells in a concentration-dependent manner through the Unc-5 netrin receptor B-focal adhesion kinase axis. *Cancer Biol. Ther.* 2023, 24, 2200705.
- [9] He XL, Cui JY, Ma H, Abuduaini N, Huang Y, Tang L, Wang WY, Zhang YY, Wang Y, Lu WQ, Feng B, Huang J. Berberrubine is a novel and selective IMPDH2 inhibitor that impairs the growth of colorectal cancer. *Biochem. Pharmacol.* 2023, 218, 115868.
- [10] Shibata M, Fukuda S, Terasaki M, Maeda H. Ishimozuku (*Sphaerotrichia firma*) lipids containing fucoxanthin suppress fatty liver and improve short chain fatty acid production in obese model mice. *Front. Sustain. Food S.* 2024, 7, 1331061.
- [11] Suwanmanee G, Tantrawatpan C, Kheolamai P, Paraoan L, Manochantr S. Fucoxanthin diminishes oxidative stress damage in human placenta-derived mesenchymal stem cells through the PI3K/Akt/Nrf-2 pathway. *Sci. Rep.* 2023, 13, 22974.
- [12] Yan J, Li ZH, Liang Y, Yang C B, Ou W, Mo HQ, Tang M, Chen DS, Zhong CB, Que DD, Feng LY, Xiao H, Song XD, Yang PZ. Fucoxanthin alleviated myocardial ischemia and reperfusion injury through inhibition of ferroptosis via the NRF2 signaling pathway. *Food Funct.* 2023, 14, 10052-10068.
- [13] Zhang XQ, Liu TY, Zhang LT, Hua ZH, Jin XA, Xu F, Ji JC, Xu BH, Ding HM. Effects and mechanisms of fucoxanthin from *Hizikia fusiforme* on inhibiting tongue squamous cell carcinoma proliferation via AKT/mTOR-mediated glycolysis. *J. Food Biochem.* 2023, 2023, 7944733.
- [14] Almeida TP, Ferreira J, Vettorazzi A, Azqueta A, Rocha E, Ramos AA. Cytotoxic activity of fucoxanthin, alone and in combination with the cancer drugs imatinib and

- doxorubicin, in CML cell lines. *Environ. Toxicol. Phar.* 2018, 59, 24-33.
- [15] Dixon SJ, Lemberg KM, Lamprecht MR, Skouta R, Zaitsev EM, Gleason CE, Patel DN, Bauer AJ, Cantley AM, Yang WS, Morrison B, Stockwell, BR. Ferroptosis: an iron-dependent form of nonapoptotic cell death. *Cell* 2012, 149, 1060-1072.
- [16] Li T, Huang HY, Qian B, Wang WH, Yuan Q, Zhang HY, He J, Ni KJ, Wang P, Zhao ZY, He JL, Fu SW, Xu L, Lin YC, Lin, ZN. Intervening mitochondrial PD-L1 suppressed IFN-gamma-induced cancer stemness in hepatocellular carcinoma by sensitizing sorafenib-induced ferroptosis. *Free Radical Bio. Med.* 2024, 212, 360-374.
- [17] Zhou TJ, Zhang MM, Liu DM, Huang LL, Yu HQ, Wang Y, Xing L, Jiang HL. Glutathione depletion and dihydroorotate dehydrogenase inhibition actuated ferroptosis-augment to surmount triple-negative breast cancer. *Biomaterials* 2024, 305, 122447.
- [18] Wang LY, Huang HM, Li XX, Ouyang LS, Wei XJ, Xie JX, Liu DX, Tan P, Hu ZD. A review on the research progress of traditional Chinese medicine with anti-cancer effect targeting ferroptosis. *Chin. Med-UK.* 2023, 18, 132.
- [19] Koeberle SC, Kipp AP, Stuppner H, Koeberle A. Ferroptosis-modulating small molecules for targeting drug-resistant cancer: Challenges and opportunities in manipulating redox signaling. *Med. Res. Rev.* 2023, 43, 614-682.
- [20] Zhou Q, Li T, Qin Q, Huang XB, Wang Y. Ferroptosis in lymphoma: Emerging mechanisms and a novel therapeutic approach. *Front. Genet.* 2022, 13, 1039951.
- [21] Kang H, Kim SC, Oh Y. Fucoxanthin abrogates ionizing radiation-induced inflammatory responses by modulating sirtuin 1 in macrophages, *Mar. Drugs* 2023, 21, 635.
- [22] Colomar-Carando N, Gauthier L, Merli P, Loiacono F, Canevali P, Falco M, Galaverna F, Rossi B, Bosco F, Caratini M, Mingari MC, Locatelli F, Vivier E, Meazza R, Pende, D. Exploiting natural killer cell engagers to control pediatric b-cell precursor acute lymphoblastic leukemia. *Cancer Immunol. Res.* 2022, 10, 291-302.
- [23] Lotfi N, Yousefi Z, Golabi M, Khalilian P, Ghezlbash B, Montazeri M, Shams MH, Baghbadorani PZ, Eskandari N. The potential anti-cancer effects of quercetin on blood, prostate and lung cancers: An update. *Front. Immunol.* 2023, 14, 1077531.
- [24] Du HF, Jin XD, Jin SZ, Zhang DL, Chen QD, Jin XA, Wang CS, Qian GY, Ding HM. Anti-Leukemia activity of polysaccharide from *Sargassum fusiforme* via the PI3K/AKT/BAD pathway in vivo and in vitro. *Mar. Drugs* 2023, 21, 289.
- [25] Wei RR, Zhao YQ, Wang J, Yang X, Li SL, Wang YY, Yang XZ, Fei JM, Hao XJ, Zhao YH, Gui LM, Ding, X. Tagitinin C induces ferroptosis through PERK-Nrf2-HO-1 signaling pathway in colorectal cancer cells. *Int. J. Bio. Sci.* 2021, 17, 2703-2717.
- [26] Zhao Y, Huang HX, Wang XN, Hu WX, Lu XF, Tang SY, Liu HN, Sun YZ. *Dendrobium officinale* polysaccharides inhibit CDCA-induced gastric intestinal metaplasia through activating NRF2/HO-1 and modulating HNF4 $\alpha$ /CDX2 signaling pathway. *J. Food Biochem.* 2023, 2023, 6668818.
- [27] Moghadamtousi SZ, Karimian H, Khanabdali R, Razavi M, Firoozinia M, Zandi K, Kadir HA. Anticancer and antitumor potential of fucoxanthin and fucoxanthin, two main metabolites isolated from brown algae. *Sci. World J.* 2014, 2014, 768323.
- [28] Ahmed SA, Mendonca P, Messeha SS, Soliman KFA. Anticancer effects of fucoxanthin through cell cycle arrest, apoptosis induction, and angiogenesis inhibition in triple-negative breast cancer cells. *Molecules*, 2023, 28, 6536.
- [29] Deng X, Liu TZ, Zhu YT, Chen JF, Song Z, Shi ZP, Chen HR. Ca & Mn dual-ion hybrid nanostimulator boosting anti-tumor immunity via ferroptosis and innate immunity awakening. *Bioact. Mater.* 2024, 33, 483-496.
- [30] Dong BW, Jiang YY, Shi BD, Zhang ZQ, Zhang ZW. Selenomethionine alleviates decabromodiphenyl ether-induced oxidative stress and ferroptosis via the NRF2/GPX4 pathway in the chicken brain. *J. Hazard. Mater.* 2024, 465, 133307.
- [31] Ferguson DT, Taka E, Tilghman SL, Womble T, Reedmond BV, Gedeon S, Flores-Rozas H, Reed SL, Soliman KFA, Kanga KJW, Darling-Reed SF. The anticancer effects of the garlic organosulfide diallyl trisulfide through the attenuation of b[a]p-induced oxidative stress, AhR expression, and DNA damage in human premalignant breast epithelial (MCF-10AT1) cells. *Int. J. Mol. Sci.* 2024, 25, 923.
- [32] Yang HY, Dai B, Chen LJ, Li YP, Jin XR, Gao CC, Han LF, Bian XL. Iberverin downregulates GPX4 and SLC7A11 to induce ferroptotic cell death in hepatocellular carcinoma cells. *Biomolecules* 2024, 14, 1407.
- [33] Wang XJ, Shen TL, Lian J, Deng K, Qu C, Li EM, Li G, Ren YW, Wang ZJ, Jiang ZD, Sun XJ, Li XQ. Resveratrol reduces ROS-induced ferroptosis by activating SIRT3 and compensating the GSH/GPX4 pathway. *Mol. Med.* 2023, 29, 137.
- [34] Kim JW, Min DW, Kim D, Kim J, Kim MJ, Lim H, Lee JY. GPX4 overexpressed non-small cell lung cancer cells are sensitive to RSL3-induced ferroptosis. *Sci. Rep-UK.* 2023, 13, 8872.
- [35] Terasaki M, Tsuruoka K, Tanaka T, Maeda H, Shibata M, Miyashita K, Kanemitsu Y, Sekine S, Takahashi M, Yagishita S, Hamada A. Fucoxanthin inhibits development of sigmoid colorectal cancer in a PDX model with alterations of growth, adhesion, and cell cycle signals. *Cancer Genom. Proteomics* 2023, 20, 686-705.
- [36] Huang YM, Jiao ZH, Fu YQ, Hou Y, Sun JX, Hu FR, Yu SZ, Gong KX, Liu YR, Zhao GS. An overview of the functions of p53 and drugs acting either on wild- or mutant-type p53. *Eur. J. Med. Chem.* 2024, 265, 116121.
- [37] Bao YN, Yang Q, Shen XL, Yu WK, Zhou L, Zhu QR, Shan QY, Wang ZC, Cao G. Targeting tumor suppressor p53 for organ fibrosis therapy. *Cell Death Dis.* 2024, 15, 336.
- [38] Rajasekaran D, Ogura J, Wachtel M, Ramachandran S, Babu E, Sivaprakasam S, Grippo PJ, Torres C, Muthusamy T, Gnana-Prakasam JP, Bhutia YD. Chronic exposure to excess iron promotes EMT and cancer via p53 loss in pancreatic cancer. *Asian J. Pharm. Sci.* 2020, 15, 237-251.

- [39] Hu CH, Zhang BY, Zhao SP. METTL3-mediated N6-methyladenosine modification stimulates mitochondrial damage and ferroptosis of kidney tubular epithelial cells following acute kidney injury by modulating the stabilization of MDM2-p53-LMN1 axis. *Eur. J. Med. Chem.* 2023, 259, 115677.
- [40] Zhu Q, Zhou YQ, Wang HX, Cao T, Wang XZ, Liu R, Wu H, Lin BY. Fucoxanthin triggers ferroptosis in glioblastoma cells by stabilizing the transferrin receptor. *Med. Oncol.* 2023, 40, 230.